

1 **Title page**

2

3 **Targeting endogenous K-RAS for degradation through the affinity-directed**
4 **protein missile system**

5

6 Sascha Röth¹, Thomas J. Macartney¹, Agnieszka Konopacka², Markus A. Queisser²
7 and Gopal P. Sapkota*¹

8

9 ¹Medical Research Council Protein Phosphorylation and Ubiquitylation Unit, University
10 of Dundee, Dundee, United Kingdom. ²GlaxoSmithKline, Protein Degradation Group,
11 Medicines Research Centre, Gunnels Wood Road, Stevenage, UK.

12 *Correspondence and requests for materials should be addressed to:

13 g.sapkota@dundee.ac.uk

14

15 Running Title: Targeted K-RAS proteolysis

16 ORCID IDs:

17 Sascha Röth: 0000-0001-7273-6701

18 Thomas J. Macartney: n.a.

19 Agnieszka Konopacka: 0000-0003-2192-1928

20 Markus A. Queisser: 0000-0002-3368-3827

21 Gopal P. Sapkota: 0000-0001-9931-3338

22

23

24

25

26 **Abstract**

27

28 For over three decades, *K-RAS* has been known as the holy grail of cancer targets,
29 one of the most frequently mutated oncogenes in cancer. Because the development
30 of conventional small molecule K-RAS inhibitors has been extremely challenging, K-
31 RAS has been dubbed as an undruggable target, and only recently a mutation specific
32 inhibitor has reached clinical trials. Targeted protein degradation has emerged as a
33 new modality in drug discovery to tackle undruggable targets. However, no degrader
34 for K-RAS has been described thus far. Our laboratory has developed an Affinity-
35 directed PROtein Missile (AdPROM) system for targeted proteolysis of endogenous
36 proteins through the ubiquitin proteasome system. Here, we show that we can achieve
37 degradation of endogenous K-RAS and H-RAS in different cell lines in a targeted
38 manner using our AdPROM system. Our findings imply that endogenous RAS proteins
39 can be targeted for proteolysis, thereby offering tantalising possibilities for an
40 alternative therapeutic approach to these so-called undruggable targets in cancer.

41

42 **Keywords**

43 High affinity binder, Ubiquitin proteasome system, UPS, Targeted proteolysis,
44 PROTAC

45

46

47

48

49

50

51 **Background**

52 The three RAS oncogenes *H-RAS*, *K-RAS* and *N-RAS*, represent the most frequently
53 mutated genes in cancer [1,2]. They encode four highly similar proteins, namely H-
54 RAS, N-RAS, K-RAS4A and K-RAS4B, which undergo C-terminal farnesylation [3,4].
55 Farnesylation, in combination with palmitoylation in the hypervariable region (HVR)
56 (N-RAS, H-RAS, K-RAS4A) or with a polybasic signal in the HVR (K-RAS4B),
57 mediates the plasma membrane interaction [5]. RAS proteins are small GTPases,
58 which cycle between the GTP-bound (active) and GDP-bound (inactive) states,
59 controlled by guanosine nucleotide exchange factors (GEF) and GTPase activating
60 proteins (GAPs) [6]. Activation of RAS proteins by various extracellular growth factors
61 initiates activation of numerous downstream signalling networks, including
62 BRAF/MAPK and PI3K pathways [7], that are critical for cell proliferation and viability.
63 Many pathogenic mutations in *RAS* genes impair GAP mediated GTP hydrolysis,
64 thereby favouring the persistence of the active RAS-GTP state, which triggers
65 constitutive activation of downstream signalling resulting in unchecked proliferation of
66 cancer cells [2,8].

67 As the oncogenicity of RAS mutations has been known for over three decades,
68 intensive efforts have been made towards drugging them. These efforts are yet to
69 result in effective RAS-inhibitor therapies [1,9]. This has promoted the perception that
70 RAS proteins are undruggable. Several factors make RAS proteins difficult targets to
71 engineer selective small molecule inhibitors. First, the relatively high concentrations of
72 GTP and GDP in cells and picomolar affinity to binding RAS proteins makes it almost
73 impossible to develop GTP/GDP analogues as inhibitors [1,10]. Second, structural
74 analysis of RAS proteins revealed few sufficiently large and deep hydrophobic pockets
75 on the surface for small molecule binding [11,12]. Recently, a covalent inhibitor

76 targeting a cysteine in K-RAS G12C was developed to target this specific mutation
77 [13]. However, these barriers and failure to directly target RAS have prompted
78 researchers to explore targeting upstream regulators, or downstream effectors of RAS
79 proteins [1,9,14–16], as well as altering levels of RAS protein, for example by inducing
80 targeted degradation of RAS [17].

81 Most targeted protein degradation approaches harness the cellular proteolytic
82 pathways that naturally maintain proteostasis, with the ubiquitin-proteasome system
83 (UPS) being frequently exploited [18]. Protein degradation by the UPS is triggered by
84 conjugation of ubiquitin chains onto the target protein, which is achieved through a
85 sequential action of three enzymes: the ubiquitin-activating enzyme (E1), which
86 activates the carboxy-terminal glycine residue of ubiquitin in an ATP-dependent
87 manner; a ubiquitin-conjugating enzyme (E2), which conjugates the activated ubiquitin
88 to its active site cysteine; and a ubiquitin ligase (E3), which facilitates the transfer of
89 ubiquitin from E2 to primarily lysine residues on substrate proteins [19,20]. Further
90 ubiquitylation on one or more lysine residues within ubiquitin then triggers
91 polyubiquitylation, followed by degradation by the proteasome [21–23]. Targeting RAS
92 for proteolysis relies on the engagement of the cellular proteolytic systems for its
93 ubiquitylation and degradation. In this context, it has been shown that the
94 heterobifunctional molecule dTAG-13, which recruits FKBP12_{F36V}-tagged proteins of
95 interest (POIs) to the CRBN/CUL4A E3 ubiquitin ligase for their degradation, can
96 degrade FKBP12_{F36V}-KRAS_{G12V} overexpressed in cell lines [17]. However,
97 FKBP12_{F36V} itself can be targeted for ubiquitylation when using heterobifunctional
98 small molecule binders [24]. Therefore, it remains unclear, whether using dTAG13 on
99 FKBP12_{F36V}-K-RAS results in the ubiquitination of K-RAS or FKBP12_{F36V}. Such
100 information is not only key to evaluate proteolysis as a druggable approach for

101 targeting RAS proteins but also to inform on the development of effective
102 heterobifunctional RAS degraders.

103 We have previously developed an effective proteolytic Affinity-directed PROtein
104 Missile (AdPROM) system for UPS mediated POI degradation [25,26]. AdPROM
105 consists of a fusion of von-Hippel-Lindau (VHL) protein, a substrate recruiter of the
106 CUL2-RING E3 ligase complex, and high-affinity binders, such as nanobodies and
107 monobodies, of POIs. Delivering AdPROM into multiple cell lines through retroviral
108 transductions led to efficient degradation of endogenous target proteins, including
109 SHP2 and ASC [26]. Furthermore, in order to target POIs for which no high-affinity
110 polypeptide binders exist, we utilized CRISPR/Cas9 genome editing to rapidly
111 introduce GFP tags on endogenous VPS34 and PAWS1 genes, and used the
112 AdPROM system consisting of anti-GFP nanobody fused to VHL to achieve near-
113 complete degradation of the endogenous GFP-VPS34 and PAWS1-GFP proteins [25].
114 In this study, we explore the use of the AdPROM system, and demonstrate its efficacy,
115 for targeted degradation of endogenously GFP-tagged K-RAS and untagged,
116 endogenous K-RAS from cells.

117

118 **Methods**

119 **Sequence Alignment**

120 Protein sequences of K-RAS4A/B, H-RAS and N-RAS were taken from Uniprot [27]
121 and aligned in Clustal Omega [28]. The alignment was further processed in JalView
122 [29] to highlight percent sequence identity.

123

124 **RNA extraction, cDNA synthesis and qRT-PCR**

125 For RNA extraction, 2×10^5 cells were seeded in a 6-well dish and harvested the next
126 day with the RNeasy Micro Kit (Qiagen, #74004) according to the manufacturer's
127 protocol. 1 μ g of RNA was reverse transcribed with the iScript cDNA synthesis Kit
128 (BIORAD, #1708891) according to the manufacturer's protocol. For qRT-PCR 1 μ l of
129 diluted cDNA (1:20 or 1:80) was mixed with forward and reverse primers (Custom
130 primers from Invitrogen, 300 nm final concentration each) and SsoFast EvaGreen
131 Supermix (BIORAD, #1725204) in a 384-well plate (Axygen, #321-22-051) and run on
132 a BIORAD CFX384.

133 Primer sequences:

134 K-RAS4A fw: GAGGGAGATCCGACAATACAG;

135 K-RAS4A rev: TCTCGAACTAATGTATAGAAGGCATC;

136 K-RAS4Bfw: TTGCCTTCTAGAACAGTAGACAC;

137 K-RAS4B rev: CATCGTCAACACCCTGTCTTG;

138 Total K-RAS fw: GGAGTACAGTGCAATGAGGG;

139 Total K-RAS rev: CCATAGGTACATCTTCAGAGTCC;

140 H-RAS fw: GAACAAGTGTGACCTGGCT;

141 H-RAS rev: ACCAACGTGTAGAAGGCATC;

142 N-RAS fw: AATACATGAGGACAGGCGAAG;

143 N-RAS rev: GTTCCCACTAGCACCATAGG;

144 GAPDH fw: CTTTGTCAAGCTCATTTCCTGG;

145 GAPDH rev: TCTTCCTCTTGTGCTCTTGC.

146 Melting curves were analysed for purity of the PCR product and fold changes were
147 calculated by the $2^{-\Delta\Delta C_t}$ method [30].

148

149 **Cell line maintenance and manipulation**

150 All cells were cultured in humidified incubators at 37°C and 5% CO₂. A549, HEK293-
151 FT, A375, A172 and SW620 cells were cultured in Dulbecco's modified Eagle's
152 medium (DMEM; Gibco) with 10% FBS (Sigma), 1% penicillin/streptomycin (Lonza)
153 and 2 mM L-glutamine (Lonza). HT-29, HPAFII and H460 cells were cultured in
154 RPMI1640 medium (Gibco), with the same supplements as DMEM. For retrovirus
155 production, 3.2 µg pCMV-gag-pol, 2.2 µg pCMV-VSV-G and 6 µg of respective
156 pBabeD plasmids were co-transfected in roughly 70% confluent HEK293-FT cells
157 cultured on a 10-cm dish. Plasmids were mixed with 600 µl Opti-MEM (Gibco) and 24
158 µl of 1 mg/ml polyethylenimine (Polysciences) dissolved in 25 mM HEPES pH 7.5.
159 The mixture was vigorously vortexed for 15 s and incubated for 20 min at room
160 temperature. The volume was adjusted to 10 ml with DMEM and added to FT cells.
161 After 24 h, medium was exchanged to DMEM or RPMI, depending on the target cell
162 growth medium. After an additional 24 h, the medium was harvested and filtered
163 through a 0.45 µm Minisart syringe filter (Sartorius). The supernatant was added to a
164 plate of roughly 70% confluent target cells in a 1:10–1:4 dilution (in respective medium)
165 in the presence of 8 µg/ml polybrene (Sigma). After 24 h, growth medium was
166 exchanged with fresh medium containing 2 µg/ml puromycin, to select transduced
167 cells. Puromycin was removed from the medium after 48 h.

168

169 Cells were lysed on ice, by washing once with PBS and scraping in lysis buffer (50
170 mM Tris–HCl pH 7.5, 0.27 M sucrose, 150 mM NaCl, 1 mM EGTA, 1 mM EDTA, 1 mM
171 sodium orthovanadate, 1 mM sodium β-glycerophosphate, 50 mM sodium fluoride, 5
172 mM sodium pyrophosphate, 1% (v/v) Triton X-100 and 0.5% Nonidet P-40)
173 supplemented with protease inhibitors (Roche; 1 tablet/25 ml of lysis buffer). Protein
174 content from cleared cell lysates was determined with Pierce Detergent Compatible

175 Bradford Assay Kit (Thermo Fisher). Lysates were processed further or frozen and
176 stored at -20°C.

177

178 **CRISPR/Cas9**

179 For generation of N-terminal GFP knock-in A549 cell lines the K-RAS locus was
180 targeted with a dual guide approach [31] (using the sense guide (pBabeD vector,
181 DU54976): GCGAATATGATCCAACAATAG; antisense guide (pX335 vector,
182 DU54980): GCTGAATTAGCTGTATCGTCA; and the GFP-KRAS donor (pMK-RQ
183 vector, DU57406). Briefly, 1 µg of each of the guideRNA plasmids and 3 µg of the
184 donor plasmid were co-transfected into A549 cells. Plasmids were mixed with 1 ml of
185 Opti-MEM (Gibco) and 20 µl of 1 mg/ml polyethyleneimine (Polysciences), vortexed
186 vigorously for 15 s and added to 70% confluent cells in a 10-cm dish. The next day,
187 cells were selected in puromycin (2.5 µg/ml) for 48 h and re-transfected with the same
188 plasmids once they reached 70% confluence. Single GFP positive cells were obtained
189 by FACS sorting and surviving single cell clones were screened by genomic DNA
190 based PCR and western blot to validate homozygous knockin of the GFP-tag on the
191 endogenous *KRAS* gene. For PCR based screening the following primers were used:
192 Fw: ATCCAAGAGAACTACTGCCATGATGC;
193 Rv: CATGACCTTCAAGGTGTCTTACAGGTC. PCR products of positive clones were
194 cloned with the StrataClone PCR Cloning Kit (Agilent) into the supplied vector system,
195 according to the manufacturer's protocol. Sequencing of positive clones was carried
196 out by the MRC-PPU DNA Sequencing and Services with a custom primer close to
197 the RAS mutation site (Rv: CAAAGAATGGTCCTGCACCAG).

198

199 **SDS PAGE and Western Blotting**

200 Cell lysates were adjusted to uniform protein concentration and mixed with 6x reducing
201 Laemmli SDS sample buffer (Fisher Scientific). 10-20 μg of total lysate protein, or
202 immunoprecipitates were resolved by SDS polyacrylamide gel electrophoresis
203 (PAGE). After PAGE, proteins were transferred onto methanol activated PVDF
204 membrane (Immobilon-P or Immobilon-FL, Merck) in Tris/glycine buffer containing
205 20% methanol in a tank blotting system for 85 min at a constant voltage of 85 V. The
206 membranes were then re-incubated with methanol for 2 minutes and stained with
207 Ponceau S solution to gauge uniform protein transfer (Sigma). After de-staining
208 membranes in TBS-T (50 mM Tris-HCl pH 7.5, 150 mM NaCl, 0.1% Tween-20), they
209 were blocked for 1 h in 5% non-fat milk (Marvel) in TBS-T. Primary antibody incubation
210 was done overnight at 4°C in 5% milk/TBS-T. Following 3x10 min washes in TBS-T,
211 membranes were incubated with respective HRP-conjugated (CST) or fluorescently
212 labelled (Biorad) secondary antibodies for 1 h, washed again 3x10 min in TBS-T and
213 developed on a ChemiDoc gel imaging system (Biorad) using the respective channels.
214 HRP-conjugated blots were incubated with Immobilon Western Chemiluminescent
215 HRP Substrate (Millipore).

216

217 **Immunoprecipitation**

218 Cell lysates were adjusted to 1 $\mu\text{g}/\mu\text{l}$ in lysis buffer. Either GFP-trap beads
219 (ChromoTek) or Anti-FLAG-M2-Affinity agarose resin (SigmaAldrich) was equilibrated
220 with lysis buffer. 300-500 μg of total protein was added to 10-15 μl of beads (50%
221 slurry) and incubated for an hour at 4°C under agitation. Centrifugation steps at 200xg
222 were done at 4°C for 2 minutes. Supernatant (flowthrough) was separated from beads,
223 and beads were washed 3-5 times in lysis buffer. Proteins were eluted in lysis buffer
224 containing Laemmli SDS sample buffer by boiling at 95°C for 5 minutes.

225

226 **Antibodies**

227 Antibodies were purchased from Thermo Fisher (Alpha tubulin, MA1-80189; rat-HRP,
228 31470), Abcam (panRAS, ab206969; HIF1a, ab1), Sigma (K-RAS4B, WH0003845M1;
229 Flag-HRP, A8592-.2MG; GFP, 11814460001) CST (GAPDH, 2118S; rabbit-HRP,
230 7074S; mouse-HRP, 7076S) and Bio-Rad (rabbit starbright 700, 12004161). Primary
231 antibodies were generally used in 1:1,000 dilutions in 5% milk TBS-T, apart from RAS
232 (1:500), and GAPDH & alpha-tubulin (1:5,000). Secondary antibodies were used in a
233 1:5,000 dilution in 5% milk TBS-T. Other primary antibodies recognizing different RAS
234 species were obtained from Proteintech (N-RAS, 10724-1-AP; H-RAS, 18295-1-AP;
235 K-RAS2B, 16155-1-AP; K-RAS2A, 16156-1-AP) and Invitrogen (H-RAS, PA5-22392;
236 K-RAS, 415700).

237 Antibodies for immunofluorescence were purchased from MBL/Caltag Medsystems
238 (GFP, 598), Abcam (ATPB, ab14730), BD Biosciences (P120 Catenin, 610133),
239 Sigma (Flag-M2, F1804) and Thermo Fisher (AlexaFluor488 [donkey anti-rabbit],
240 A21206; AlexaFluor594 [goat anti-mouse], A11005).

241

242 **Immunofluorescence**

243 Cells were seeded in a 12-well dish onto cover slips and grown over night. The next
244 day, cells were washed twice in PBS and fixed for 10 minutes in 4%
245 formaldehyde/PBS (Sigma). Coverslips were washed in DMEM (Gibco) containing 10
246 mM HEPES followed by a 10 min incubation. Coverslips were washed in PBS and
247 permeabilised for 3 min in either 0.2% NP-40/PBS or 0.2% Triton X-100/PBS.
248 Coverslips were washed twice in PBS and blocked for 15 min in 3% BSA (Sigma) in
249 PBS. Primary antibody incubation was done for 1-2 h at room temperature at

250 appropriate antibody dilutions in blocking solution. Residual antibody was washed
251 away in 0.2% Tween/PBS (3x10 min). Secondary antibody incubation was done for
252 30 min at 1:300 antibody dilution in the dark. The same wash steps were repeated,
253 but the first wash contained DAPI (0.5–1 μ g in 10 ml). Finally, coverslips were dipped
254 in water, air dried and mounted on slides with Vectashield (Vector Laboratories).
255 Fluorescence signals were analysed on a Deltavision Widefield microscope (GE).
256 Images were deconvolved using the default settings of softWoRx Imaging software.
257

258 **Cell Proliferation Assays**

259 After trypsinization, live cell numbers were determined in a Neubauer haemocytometer
260 in the presence of trypan blue. Cell numbers were adjusted to 5000 cells per ml in the
261 respective growth medium. 5000 cells were added per well of a 12-well dish, and each
262 line was grown in triplicates. After 7 days, relative cell numbers were determined by
263 crystal violet staining. In short, cells were washed in PBS, fixed for 5 min in fixing buffer
264 (10% methanol, 10% acetic acid), washed in PBS again and incubated for 30-60 min
265 in crystal violet solution (0.5% crystal violet in 20% methanol). Plates were dipped in
266 tap water to remove stain and air dried overnight. Plates were scanned on a Licor
267 Odyssey using the 700 nm channel. Subsequently, 1 ml methanol was added to each
268 well and plates were incubated shaking for 30 min. Depending on the colour of 1 set
269 of cells, 100-200 μ l of supernatant was loaded in triplicate on a 96-well plate and
270 absorbance at 570 nm was measured in an Epoch microplate spectrophotometer
271 (BioTek). Values were normalized to the untreated sample and a one-way ANOVA
272 analysis with Dunnett's multiple comparisons test was done.

273

274 **Flow Cytometric Analysis**

275 Cells were trypsinized, washed and resuspended in PBS containing 1% FBS. Cells
276 were then analysed on a FACS Canto II flow cytometer. Cells were analysed with the
277 following gating strategy: (i) cells: in a plot of FSC-A vs. SSC-A, a gate was drawn
278 surrounding the major population of cells, removing debris and dead cells. (ii) single
279 cells: in a plot of FSC-A vs. FSC-W, a gate was drawn around an area corresponding
280 to single cells. (iii) in the 'single cells' population on a GFP-A vs. PE-A plot a gate was
281 drawn around GFP-positive cells in A549_{GFPKRAS} sample, using WT A549 cells as a
282 negative control. Gates (i) and (ii) were adjusted to the individual cell lines. Gate (iii)
283 was kept unchanged within an experiment.

284

285 **Results**

286 **Generation of a GFP-KRAS knock-in non-small cell lung cancer A549 cell line**

287 The high degree of amino acid sequence similarity between the four RAS proteins, i.e.
288 K-RAS4A, K-RAS4B, H-RAS and N-RAS (Fig. 1A), and the subsequent difficulty in
289 generating selective antibodies against individual isoforms pose substantial
290 challenges in studying specific RAS proteins [32]. In order to explore targeted
291 proteolysis of K-RAS using the AdPROM system, we employed CRISPR/Cas9
292 technology to generate an A549 non-small cell lung carcinoma (NSCLC) cell line
293 harbouring a homozygous knock-in of green fluorescent protein (GFP) cDNA at the N-
294 terminus of the native *K-RAS* gene (Fig. S1). As K-RAS4A and K-RAS4B are splice
295 variants differing only in their extreme C-terminus (Fig. 1A), this approach allowed us
296 to simultaneously tag both isoforms with GFP. The homozygous GFP knock-ins on
297 the native K-RAS locus (A549_{GFPKRAS}) were verified by genomic sequencing (Fig. S1).
298 Moreover, by western blot analysis using both pan-RAS and K-RAS4B antibodies, the
299 appearance of higher molecular weight GFP-K-RAS species with a concurrent

300 disappearance of the native molecular weight K-RAS species was evident in the
301 A549^{GFPKRAS} cell line compared to wild type (WT) A549 control cells (Fig. 1B). The use
302 of a panRAS antibody resulted in the detection of two distinct bands in A549 WT cells
303 (Fig.1B). As the lower band remained intact in A549^{GFPKRAS} cells, it most likely
304 corresponds to H- and/or N-RAS (Fig. 1B). However, in A549 cells we were unable to
305 detect any endogenous signals with commercially available H-RAS, N-RAS or K-
306 RAS4A specific antibodies (listed in Methods section). By qRT-PCR, we showed that
307 levels of H- and N-RAS transcripts were slightly reduced in A549^{GFPKRAS} cells
308 compared to WT A549 cells, while transcript levels of K-RAS were reduced by roughly
309 50% (Fig. S2). We were able to efficiently immunoprecipitate GFP-K-RAS from
310 A549^{GFPKRAS} but not WT A549 cell extracts (Fig. 1C).

311
312 Recently, a number of RAS antibodies have been evaluated for selective recognition
313 of the different RAS proteins by Western blotting [32], but none of these have been
314 selective for use in immunofluorescence studies. Consequently, studies evaluating
315 subcellular distribution of RAS proteins have been restricted to overexpression
316 systems. Validation of A549^{GFPKRAS} cells allowed us to investigate the sub-cellular
317 distribution of endogenous GFP-K-RAS driven by the native promoter. Endogenous
318 GFP-K-RAS displayed predominantly plasma membrane distribution, which was
319 confirmed by co-staining with P120 catenin, which is known to localise to the plasma
320 membrane [33] (Fig. 1D, Fig. S3). Additionally, we also observed some weak
321 cytoplasmic localisation of GFP-K-RAS. However, no co-localisation of GFP-K-RAS
322 was observed with mitochondrial marker ATPB [34] (Fig. 1D, Fig. S3).

323

324 **Targeted degradation of GFP-K-RAS by the proteolytic AdPROM system**

325 We sought to test whether endogenously expressed GFP-K-RAS protein in
326 A549^{GFPKRAS} cells could be targeted for degradation by AdPROM [25,26]. We have
327 previously shown that fusion of VHL to an aGFP16 nanobody recruits GFP-tagged
328 proteins, such as VPS34 and PAWS1, to the CUL2-RBX1 E3 ligase machinery for
329 target ubiquitination and subsequent proteasomal degradation [25]. Therefore, we
330 postulated that GFP-K-RAS could be recruited in a similar manner to the CUL2-RBX
331 complex for ubiquitination and degradation (Fig. 2A). Indeed, expression of VHL-
332 aGFP16 AdPROM resulted in near complete clearance of GFP-K-RAS from
333 A549^{GFPKRAS} cells compared to the untransduced controls, while the low molecular
334 weight band corresponding to H- and/or N-RAS was unaffected (Fig. 2B). In contrast,
335 neither VHL nor the aGFP16 nanobody alone, serving as controls, caused any
336 apparent changes in the steady state levels of GFP-K-RAS or other RAS proteins (Fig.
337 2B). Treatment of VHL-aGFP16 AdPROM expressing A549^{GFPKRAS} cells with the Cullin
338 neddylation inhibitor MLN4924 partially rescued the degradation of GFP-K-RAS
339 compared to DMSO-treated controls (Fig. 2C). The neddylation of CUL2 allows a
340 conformational change of the CUL2-RBX E3 ligase machinery so that the RBX E3
341 ligase is able to ubiquitinate substrates recruited by VHL. In line with this notion, the
342 levels of HIF1 α protein, a *bona fide* substrate of VHL [35], were stabilized upon
343 MLN4924 treatment compared to DMSO control (Fig. 2C). Despite the high apparent
344 efficiency of GFP-KRAS degradation by VHL-aGFP16 AdPROM, the retroviral
345 transduction of A549^{GFPKRAS} cells often generates uneven levels of AdPROM
346 expression in a mixed population of cells. Therefore, in order to get a better
347 understanding of the distribution of the cells within this population, we employed a flow
348 cytometric analysis based on GFP fluorescence. We employed gates to define a GFP-
349 positive population based on the GFP-signal from untransduced A549^{GFPKRAS} cells and

350 using WT A549 cells as a GFP-negative control (Fig. 2D). In accordance with the
351 Western blot results (Fig. 2B), 97% of cells expressing VHL-aGFP16 AdPROM
352 showed GFP-KRAS degradation compared to untransduced A549_{GFPKRAS} cells (Fig.
353 2D), which manifested in an overall reduction of GFP fluorescence of the single cell
354 population (Fig. 2E). The remaining 3% of A549_{GFPKRAS} cells produced GFP signal
355 comparable to untransduced GFP-positive-population, which could be due to low level
356 AdPROM expression within these cells (Fig. 2D). In contrast, A549_{GFPKRAS} cells
357 expressing VHL or aGFP16 alone were defined as GFP-positive at 99.3% or 99.8%,
358 respectively (Fig. 2D, E).

359

360 **AdPROM mediated degradation of endogenous RAS proteins**

361 The AdPROM-mediated degradation of GFP-K-RAS in A549_{GFPKRAS} cells
362 demonstrated the prospect of targeted degradation of endogenous K-RAS. However,
363 the presence of the GFP-tag raised the possibility of ubiquitination occurring on the
364 GFP moiety, instead of on K-RAS. Therefore, we sought to explore whether we could
365 exploit the AdPROM system to degrade endogenous, unmodified K-RAS from A549
366 cells. At present, there are no reported high affinity, selective polypeptide binders of
367 K-RAS. However, we utilized an anti-H-RAS (aHRAS) monoclonal antibody that was reported to
368 bind and immunoprecipitate both H-RAS and K-RAS, but not N-RAS [36]. Using this
369 monoclonal antibody with a FLAG-tag, we showed that anti-FLAG immunoprecipitates (IPs)
370 could robustly coprecipitate both GFP-tagged and untagged K-RAS, as well as the
371 lower molecular weight protein representing the H- and/or N-RAS band but most likely
372 to be H-RAS [36] (Fig. 3A). However, neither RAS protein was completely depleted
373 from flow-through extracts, suggesting incomplete immunoprecipitation (Fig. 3A). In

374 contrast, anti-FLAG IPs from extracts expressing Flag-VHL control did not co-
375 precipitate either protein (Fig. 3A).

376

377 Next, we sought to investigate whether AdPROM consisting of VHL fused to aHRAS
378 monobody could target K- and H-RAS proteins for degradation. In A549^{GFPKRAS} cells,
379 the expression of VHL-aHRAS resulted in a strong reduction of the GFP-K-RAS
380 protein levels when compared to untransduced, VHL or monobody alone controls (Fig.
381 3B). However, the degradation induced by VHL-aHRAS AdPROM was slightly less
382 efficient than that achieved with the VHL-aGFP16 AdPROM (Fig. 3B). Unlike VHL-
383 aGFP16, VHL-aHRAS also reduced the protein levels corresponding to the H-RAS
384 and/or N-RAS band (Fig. 3B). The loss in protein levels of endogenous H-RAS protein
385 caused by VHL-aHRAS AdPROM could be rescued by the Cullin neddylation inhibitor
386 MLN4924, suggesting that the degradation was mediated through CUL2-RBX E3
387 ligase machinery (Fig. 3C). As expected, MLN4924 also stabilised endogenous HIF1 α
388 (Fig. 3C). We also assessed the relative abundance of GFP-K-RAS in mixed
389 populations of A549^{GFPKRAS} cells transduced with VHL-aHRAS AdPROM in
390 comparison to controls by flow cytometry. We found that 77% of cells showed
391 degradation of GFP-K-RAS, as assessed by the shift of the GFP-positive gated
392 population towards the GFP-negative population (Fig. 3D) and the overall reduction of
393 GFP-signal (Fig. 3E). The remaining 23% of cells transduced with VHL-aHRAS were
394 seemingly unaffected in both positioning in the GFP-positive gate (Fig. 3D), as well as
395 GFP intensity (Fig. 3E). Transductions with VHL or aHRAS alone did not induce a
396 noticeable shift of the GFP population or GFP signal intensity (Fig. 3D & E).

397

398 Uneven retroviral transduction of cells could result in unequal expression of the
399 AdPROM constructs in different cells resulting in a mixed, divergent cell population,
400 which may account for the apparent uneven degradation of GFP-K-RAS through VHL-
401 aHRAS. When we analysed these A549^{GFPKRAS} mixed cell populations by
402 immunofluorescence for GFP signal, in untransduced and aHRAS-transduced control
403 cells, a predominant plasma membrane GFP-K-RAS signal was evident (Fig. 3F).
404 Transduction of A549^{GFPKRAS} cells with either VHL-aHRAS or VHL-aGFP16 AdPROM
405 produced a heterogenous population comprising cells with missing or severely
406 attenuated GFP signal, and cells with intact GFP-K-RAS staining pattern, localizing
407 mainly to the plasma membrane (Fig. 3F). In contrast, we noticed a slight increase in
408 perinuclear GFP-K-RAS signal in cells transduced with the aHRAS monobody alone
409 (Fig. 3F). Interestingly, we detected that the majority of the monobody itself was in the
410 nucleus (Fig. S4), while we were unable to consistently detect signals for the AdPROM
411 fusion proteins by anti-FLAG immunofluorescence (Fig. S4).

412

413 We also tested the degradation of endogenous K- and H-RAS in WT A549 cells with
414 VHL-aHRAS AdPROM. The transduction of cells with VHL-aHRAS resulted in a
415 substantial reduction in apparent levels of both K-RAS (upper band) and H-RAS (lower
416 band) proteins as detected by the pan-RAS antibody compared to untransduced
417 controls (Fig. 3G). Unlike in A549^{GFPKRAS} cells (Fig. 3B), WT cells transduced with
418 VHL-aGFP16 AdPROM did not have any noticeable effect on K-RAS and H-RAS
419 protein levels relative to untransduced cells (Fig. 3G), further validating the targeted
420 nature of RAS degradation by AdPROM. Cells transduced with the aHRAS monobody
421 alone led to a slight increase in abundance of both K-RAS and H-RAS proteins
422 compared to untransduced controls (Fig. 3G). We sought to explore whether targeted

423 degradation of K- and H-RAS proteins from WT A549 cells using the VHL-aHRAS
424 AdPROM, and GFP-K-RAS from A549^{GFPKRAS} cells using the VHL-aGFP16 AdPROM
425 would impact cell proliferation. No significant differences in proliferation could be
426 observed for either WT A549 or A549^{GFPKRAS} cells following AdPROM-mediated
427 degradation of the respective RAS proteins compared to controls after 7 days, as
428 measured by crystal violet staining (Figs. 3H & I). Although A549 cells harbour the
429 oncogenic K-RAS_{G12S} mutation, they also harbour over 250 genetic mutations
430 (COSMIC cell lines project), including some known oncogenes and tumour
431 suppressors reducing the likelihood that these cells are solely dependent on the K-
432 RAS_{G12S} oncogene for their proliferation.

433

434 **Expansion of the RAS-targeting AdPROM system in different cell lines**

435 Having demonstrated for the first time that the VHL-aHRAS AdPROM system could
436 target endogenous H- and K-RAS for degradation in A549 cells, we sought to explore
437 whether the system would work in other cell lines. First, we compared different cell
438 lines for their endogenous RAS protein expression (Fig. 4A) relative to A549 cells. All
439 cells tested displayed K-RAS protein expression similar to or slightly lower than A549
440 cells. SW620 cells, which harbour the G12V mutation on K-RAS [37], displayed similar
441 levels of expression to A549 cells, however, we noticed that K-RAS in this cell line
442 produced a slight but noticeable molecular weight shift, when probed with panRAS
443 and K-RAS4B antibodies (Fig. 4A). Protein levels corresponding to the lower H- and/or
444 N-RAS band were similar in all lines tested but overall much lower in intensity than
445 that seen for K-RAS. We tested the ability of VHL-aHRAS AdPROM to degrade RAS
446 proteins from HT-29 and SW620 cells. In HT-29 cells, which express WT RAS proteins
447 but harbour the activating BRAF V600E mutation [38], only the levels of H-RAS but

448 not K-RAS proteins were reduced by VHL-aHRAS AdPROM compared to controls
449 (Fig. 4B, left panel). The proliferation of HT-29 cells was only reduced by about 50%
450 by the aHRAS monobody alone (Fig. 4C and D), while the VHL-aHRAS and VHL-
451 aGFP16 constructs reduced growth to a lesser extent (Fig. 4D, left panel). For SW620
452 cells, which harbour the G12V mutation of K-RAS, we noticed a high K-RAS signal to
453 H-/N-RAS signal ratio, as the latter was barely detectable (Fig. 4B, right panel). We
454 observed stabilization of K-RAS with the aHRAS monobody alone, while VHL-aHRAS
455 failed to degrade K-RAS compared to controls. Interestingly, both the aHRAS
456 monobody alone and the VHL-aHRAS AdPROM but not VHL-aGFP16 AdPROM were
457 able to reduce the proliferation of SW620 cells significantly by about 50% (Fig. 4C &
458 D).

459

460 **Discussion**

461 In this report, we demonstrate that endogenous K-RAS and H-RAS proteins can be
462 targeted for degradation using the proteolytic AdPROM system. RAS proteins have
463 remained elusive targets for anti-cancer therapies, primarily due to their undruggability
464 [1]. Research into obtaining small molecule inhibitors of K-RAS has been carried out
465 for over 30 years without much success [39]. Recently, RAS targeting small molecules
466 have emerged, with specificities to (i) a specific mutation status of K-RAS (G12C), i.e.
467 ARS-1620 [40], and ARS-853 [41]; (ii) K-RAS, independent of the mutation status [42];
468 or (iii) RAS proteins in either nucleotide binding state [43]. Two compounds targeting
469 K-RAS_{G12C} mutation, AMG510 and MRTX849, are currently undergoing clinical trials
470 [44]. An alternative approach has been the development of high affinity polypeptide
471 binders of RAS that neutralise the RAS function. A class of binders based on ankyrin
472 repeat proteins (DARPINs) [45] can bind and neutralise specific nucleotide loading

473 states of RAS proteins [45]. Similarly, a fibronectin type III domain-based RAS-binding
474 monobody [36,46–48] was shown to bind and inhibit the dimerization of both K- and
475 H-RAS, and the overexpression of this monobody was shown to suppress tumour
476 growth in mice [48]. Besides inhibition, RAS degradation offers another alternative
477 approach at inhibiting RAS function to target RAS-dependent cancer cells. In this
478 context, the dTAG-13 PROTAC was used to degrade FKBP12_{F36V}-tagged K-RAS [17]
479 through the UPS, albeit when overexpressed in cells. Our AdPROM system,
480 demonstrating here that endogenous RAS proteins can be targeted for proteolysis
481 through the UPS, informs that small molecules targeting RAS proteins for degradation
482 is a viable option for intervention. Furthermore, our A549_{GFPKRAS} cells provide an
483 excellent high throughput screening platform to test the efficacy of such molecules.
484 However, targeted delivery of polypeptide binders of RAS proteins or the proteolytic
485 AdPROM system into RAS-dependent cancer cells remains challenging and therefore
486 currently offers limited therapeutic potential.

487

488 One difficulty in the study of RAS proteins is the absence of robust reagents to reliably
489 detect specific RAS proteins at the endogenous levels, especially by
490 immunofluorescence [32]. Often, overexpression of GFP-tagged or other epitope-
491 tagged K-RAS has been employed to investigate RAS localization [36,49,50].
492 Therefore, our homozygous A549_{GFPKRAS} NSCLC cell line generated using
493 CRISPR/Cas9, notwithstanding the potential caveats of GFP-tagging, has allowed us
494 to not only assess localization of endogenously driven GFP-K-RAS protein but its
495 mobility shift has allowed us to test the utility of panRAS and K-RAS antibodies in
496 detecting K-RAS by Western blotting. Beyond the plasma membrane localisation, we
497 observed additional disperse cytoplasmic signals of endogenous GFP-K-RAS, but no

498 mitochondrial localisation. When overexpressed, K-RAS_{G12V} has been implied to be
499 transported into mitochondria, leading to alterations of membrane potential, a
500 decrease in respiration and an increase in glycolysis [51]. Potential compartments for
501 the observed cytosolic signal for K-RAS could be Golgi, as seen for H- and N-RAS
502 [52], which could correspond to K-RAS4A signal, or Endoplasmic Reticulum. However,
503 this remains to be verified.

504

505 While the VHL-aGFP AdPROM was very effective at selectively degrading GFP-K-
506 RAS from A549_{GFPKRAS} cells, the VHL-aHRAS AdPROM degraded endogenous H-
507 and K-RAS with mixed efficacy in different cell lines. In developing the aHRAS
508 monobody, the authors noted a difference in downstream behaviours of H- and K-RAS
509 upon monobody binding, such as K-RAS, but not H-RAS being displaced from the
510 membrane, or the mutant K-RAS, but not mutant H-RAS interaction with RAF being
511 disturbed by monobody binding [46]. The full determinants of interaction between the
512 aHRAS monobody and different H- and K-RAS mutants or any post-translationally
513 modified forms remain poorly defined. It is perhaps the differences in affinity between
514 the RAS proteins and the aHRAS monobody that define how robustly or poorly VHL-
515 aHRAS can degrade different RAS proteins. Nonetheless, our study proves that any
516 high-affinity polypeptide binders that can selectively bind specific RAS proteins or
517 mutants can be packaged with VHL-AdPROM in order to target specific RAS proteins
518 for proteasomal degradation. We also noted that aHRAS monobody alone resulted in
519 a marked stabilization of both H-RAS and K-RAS in multiple cells (Fig. 3G & F and
520 Fig. 4B), which could be caused either by a feedback loop induced by the inhibition of
521 both RAS species imparted by aHRAS binding, or by blocking the natural turnover

522 pathway through binding the RAS dimerization interface at helical structures $\alpha 4$ - $\alpha 5$
523 [36].

524

525 For the cell lines that we used, AdPROM-mediated degradation of H-/K-RAS was not
526 sufficient to induce inhibition of anchorage-dependent cell proliferation. For A549 cells
527 that are considered not to be K-RAS-dependent for proliferation, this is perhaps not
528 surprising [53,54]. Meanwhile, SW620 cells have been reported to be K-RAS
529 dependent for proliferation [55], however, their proliferation was inhibited by aHRAS
530 monobody alone and the VHL-aHRAS AdPROM, which caused no detectable
531 degradation of K-RAS, did not inhibit their proliferation any further. The inhibition of
532 cell proliferation of RAS-dependent cells by aHRAS monobody is consistent with
533 previous reports [36,48]. The lack of degradation of K-RAS by VHL-aHRAS AdPROM
534 could be due to the unusual size shift of K-RAS in these cells, possibly caused by a
535 post-translational modification or a mutation that might allow binding to aHRAS
536 monobody but prevent ubiquitylation by the VHL-AdPROM, although this needs to be
537 defined further. Many RAS-dependent cell proliferation assays employ anchorage-
538 independent 3D cultures. For example, the K-RAS_{G12C} drug ARS-1620 was shown to
539 be effective at inhibiting RAS-dependent cell proliferation in 3D cultures but not in 2D
540 cultures [40]. In order to assess the effects of AdPROM-mediated degradation of H-
541 /K-RAS on proliferation robustly, it will be essential to first obtain polypeptide RAS
542 binders that bind to specific RAS proteins with high affinity and then use them in RAS-
543 dependent cell lines using 3D proliferation assays.

544

545 Recently two allosteric small molecule binders were described for K-RAS with low
546 micromolar and nanomolar binding affinities [42,43]. It would be important to test these

547 binders' capabilities as K-RAS targeting warheads in a PROTAC approach. In this line,
548 a re-evaluation of RAS binding molecules, with or without inhibitory function, might
549 prove successful for PROTAC designs.

550

551 **Conclusion**

552 Our findings demonstrate clearly that endogenous RAS proteins can be targeted for
553 proteasomal degradation by employing the AdPROM system. The system is not only
554 suitable for studying the functions of these RAS proteins but also unequivocally
555 informs that targeted proteolysis of endogenous K-RAS is a viable strategy to target
556 K-RAS-dependent pathologies. The findings open up exciting opportunities to develop
557 VHL-recruiting K-RAS-specific cell-permeable PROTACs as potential therapeutic
558 agents. Our findings also highlight the need for developing better and more selective
559 RAS binding polypeptides, such as nanobodies or monobodies, to achieve more
560 selective degradation with the AdPROM system.

561

562 **List of abbreviations**

563 AdPROM – Affinity directed PROtein Missile

564 ASC – Apoptosis-associated speck-like protein containing a CARD

565 ATPB – ATP synthase subunit β

566 BRAF – B – Rapidly Accelerated Fibrosarcoma

567 Cas9 – CRISPR associated protein 9

568 CRBN – Cereblon

569 CRISPR – Clustered Regularly Interspaced short palindromic repeats

570 CUL – Cullin

571 DAPI – 4,6-diamidino-2-phenylindole

- 572 DARPIN – Designed Ankyrin Repeat Protein
- 573 FACS – Fluorescence Activated Cell Sorting
- 574 FKBP – FK506 Binding Protein
- 575 GAP – GTPase Activating Protein
- 576 GAPDH – Glyceraldehyde 3-phosphate dehydrogenase
- 577 GDP – Guanosine diphosphate
- 578 GEF – Guanosine Nucleotide Exchange Factor
- 579 GFP – Green Fluorescent Protein
- 580 GTP – Guanosine triphosphate
- 581 HIF1 α - Hypoxia Inducible Factor 1 α
- 582 HVR – Hypervariable region
- 583 MAPK – Mitogen Activated Protein Kinase
- 584 NSCLC – Non-small cell lung carcinoma
- 585 PAWS1 – Protein associated with Smad1
- 586 PI3K – Phosphoinositide 3-kinase
- 587 qRT-PCR – Real-time quantitative RT-PCR
- 588 RAS – Rat Sarcoma
- 589 RBX1 – RING box protein 1
- 590 SDS-PAGE – SDS Polyacrylamide Gel Electrophoresis
- 591 SHP2 – Src homology region 2 (SH2)-containing protein tyrosine phosphatase 2
- 592 UPS – Ubiquitin Proteasome System
- 593 VHL – Von-Hippel-Lindau
- 594 VPS34 – Vacuolar protein sorting 34
- 595
- 596 **Declarations**

597 **Ethics approval and consent to participate**

598 Not applicable

599 **Consent for publication**

600 Not applicable

601 **Availability of data and materials**

602 All data generated and analysed during this study is currently available in the Center
603 for Open Science repository under the following link,
604 https://osf.io/g5qn9/?view_only=4ef0cf7df11f4174b5f6760fa10042fe

605 Data will be stored as permanent registry and publicly available upon acceptance of
606 the manuscript.

607 **Competing interests**

608 The authors declare that they have no competing interests

609 **Funding**

610 SR is supported by GlaxoSmithKline through the Division of Signal Transduction
611 Therapy collaboration. AK and MQ are employees of GlaxoSmithKline. GPS is
612 supported by the UK MRC (Grant MC_UU_12016/3) and the pharmaceutical
613 companies supporting the Division of Signal Transduction Therapy (Boehringer-
614 Ingelheim, GlaxoSmithKline, Merck-Serono).

615 **Authors' contributions**

616 TJM generated all used plasmids. SR, AK, MAQ and GPS designed the project. SR
617 and GPS drafted the manuscript. SR acquired and analysed the data. SR and GPS
618 interpreted the data.

619 **Acknowledgements**

620 We thank GS laboratory members for their highly appreciated experimental advice
621 and/or discussions during the course of these experiments. We thank L. Fin, E. Allen,

622 J. Stark and A. Muir for help and assistance with tissue culture, the staff at the DNA
623 Sequencing services (School of Life Sciences, University of Dundee), and the cloning
624 teams within the MRC-PPU reagents and services (University of Dundee), coordinated
625 by J. Hastie and H. McLauchlan. We thank the staff at the Dundee Imaging Facility
626 (School of Life Sciences, University of Dundee), and the staff at the flow cytometry
627 facility (School of Life Sciences, University of Dundee) for their invaluable help and
628 advice throughout this project.

629

630 **References**

- 631 [1] Cox AD, Fesik SW, Kimmelman AC, Luo J, Der CJ. Drugging the undruggable
632 RAS: Mission Possible? *Nat Rev Drug Discov* 2014;13:828–51.
633 doi:10.1038/nrd4389.
- 634 [2] Hobbs GA, Der CJ, Rossman KL. RAS isoforms and mutations in cancer at a
635 glance. *J Cell Sci* 2016;129:1287–92. doi:10.1242/jcs.182873.
- 636 [3] Schaber MD, O’Hara MB, Garsky VM, Mosser SD, Bergstrom JD, Moores SL,
637 et al. Polyisoprenylation of Ras in Vitro by a Farnesyl-Protein Transferase. *J*
638 *Biol Chem* 1990;265:14701–4.
- 639 [4] Reiss Y, Goldstein JL, Seabra MC, Casey PJ, Brown MS. Inhibition of purified
640 p21ras farnesyl:protein transferase by Cys-AAX tetrapeptides. *Cell*
641 1990;62:81–8. doi:10.1016/0092-8674(90)90242-7.
- 642 [5] Ahearn IM, Haigis K, Bar-Sagi D, Philips MR. Regulating the regulator: post-
643 translational modification of RAS. *Nat Rev Mol Cell Biol* 2012;13:39–51.
644 doi:10.1038/nrm3255.
- 645 [6] Vigil D, Cherfils J, Rossman KL, Der CJ. Ras superfamily GEFs and GAPs:
646 validated and tractable targets for cancer therapy? *Nat Rev Cancer*

- 647 2010;10:842–57. doi:10.1038/nrc2960.
- 648 [7] Khan AQ, Kuttikrishnan S, Siveen KS, Prabhu KS, Shanmugakonar M, Al-
649 Naemi HA, et al. RAS-mediated oncogenic signaling pathways in human
650 malignancies. *Semin Cancer Biol* 2019;54:1–13.
651 doi:10.1016/j.semcancer.2018.03.001.
- 652 [8] Marcus K, Mattos C. Direct Attack on RAS: Intramolecular Communication and
653 Mutation-Specific Effects. *Clin Cancer Res* 2015;21. doi:10.1158/1078-
654 0432.CCR-14-2148.
- 655 [9] Papke B, Der CJ. Drugging RAS: Know the enemy. *Science* 2017;355:1158–
656 63. doi:10.1126/science.aam7622.
- 657 [10] John J, Sohmen R, Feuerstein J, Linke R, Wittinghofer A, Goody RS. Kinetics
658 of interaction of nucleotides with nucleotide-free H-ras p21. *Biochemistry*
659 1990;29:6058–65. doi:10.1021/bi00477a025.
- 660 [11] O'Bryan JP. Pharmacological targeting of RAS: Recent success with direct
661 inhibitors. *Pharmacol Res* 2019;139:503–11. doi:10.1016/j.phrs.2018.10.021.
- 662 [12] Pai EF, Kabsch W, Krengel U, Holmes KC, John J, Wittinghofer A. Structure of
663 the guanine-nucleotide-binding domain of the Ha-ras oncogene product p21 in
664 the triphosphate conformation. *Nature* 1989;341:209–14.
665 doi:10.1038/341209a0.
- 666 [13] Ostrem JM, Peters U, Sos ML, Wells JA, Shokat KM. K-Ras(G12C) inhibitors
667 allosterically control GTP affinity and effector interactions. *Nature*
668 2013;503:548–51. doi:10.1038/nature12796.
- 669 [14] Leung ELH, Luo LX, Liu ZQ, Wong VKW, Lu LL, Xie Y, et al. Inhibition of
670 KRAS-dependent lung cancer cell growth by deltarasin: blockage of autophagy
671 increases its cytotoxicity. *Cell Death Dis* 2018;9:216. doi:10.1038/s41419-017-

- 672 0065-9.
- 673 [15] Waldmann H, Karaguni I-M, Carpintero M, Gourzoulidou E, Herrmann C,
674 Brockmann C, et al. Sulindac-Derived Ras Pathway Inhibitors Target the Ras–
675 Raf Interaction and Downstream Effectors in the Ras Pathway. *Angew Chemie*
676 *Int Ed* 2004;43:454–8. doi:10.1002/anie.200353089.
- 677 [16] Kang S, Kim E-S, Moon A. Simvastatin and lovastatin inhibit breast cell
678 invasion induced by H-Ras. *Oncol Rep* 2009;21:1317–22.
679 doi:10.3892/or_00000357.
- 680 [17] Nabet B, Roberts JM, Buckley DL, Paulk J, Dastjerdi S, Yang A, et al. The
681 dTAG system for immediate and target-specific protein degradation. *Nat Chem*
682 *Biol* 2018;14:431–41. doi:10.1038/s41589-018-0021-8.
- 683 [18] Röth S, Fulcher LJ, Sapkota GP. Advances in targeted degradation of
684 endogenous proteins. *Cell Mol Life Sci* 2019;76:2761–77. doi:10.1007/s00018-
685 019-03112-6.
- 686 [19] Pickart CM, Eddins MJ. Ubiquitin: structures, functions, mechanisms. *Biochim*
687 *Biophys Acta* 2004;1695:55–72. doi:10.1016/j.bbamcr.2004.09.019.
- 688 [20] Roos-Mattjus P, Sistonen L. The ubiquitin-proteasome pathway. *Ann Med*
689 2004;36:285–95.
- 690 [21] Komander D, Rape M. The Ubiquitin Code. *Annu Rev Biochem* 2012;81:203–
691 29. doi:10.1146/annurev-biochem-060310-170328.
- 692 [22] Yau R, Rape M. The increasing complexity of the ubiquitin code. *Nat Cell Biol*
693 2016;18:579–86. doi:10.1038/ncb3358.
- 694 [23] Akutsu M, Dikic I, Bremm A. Ubiquitin chain diversity at a glance. *J Cell Sci*
695 2016;129:875–80. doi:10.1242/jcs.183954.
- 696 [24] Winter GE, Buckley DL, Paulk J, Roberts JM, Souza A, Dhe-Paganon S, et al.

- 697 Phthalimide conjugation as a strategy for in vivo target protein degradation.
698 Science 2015;348:1376–81. doi:10.1126/science.aab1433.
- 699 [25] Fulcher LJ, Macartney T, Bozatz P, Hornberger A, Rojas-Fernandez A,
700 Sapkota GP. An affinity-directed protein missile system for targeted
701 proteolysis. Open Biol 2016;6. doi:10.1098/rsob.160255.
- 702 [26] Fulcher LJ, Hutchinson LD, Macartney TJ, Turnbull C, Sapkota GP. Targeting
703 endogenous proteins for degradation through the affinity-directed protein
704 missile system. Open Biol 2017;7. doi:10.1098/rsob.170066.
- 705 [27] The UniProt Consortium. UniProt: a worldwide hub of protein knowledge.
706 Nucleic Acids Res 2019;47:D506–15. doi:10.1093/nar/gky1049.
- 707 [28] Madeira F, Park YM, Lee J, Buso N, Gur T, Madhusoodanan N, et al. The
708 EMBL-EBI search and sequence analysis tools APIs in 2019. Nucleic Acids
709 Res 2019;47:W636–41. doi:10.1093/nar/gkz268.
- 710 [29] Waterhouse AM, Procter JB, Martin DMA, Clamp M, Barton GJ. Jalview
711 Version 2 - a multiple sequence alignment editor and analysis workbench.
712 Bioinformatics 2009;25:1189–91. doi:10.1093/bioinformatics/btp033.
- 713 [30] Livak KJ, Schmittgen TD. Analysis of Relative Gene Expression Data Using
714 Real-Time Quantitative PCR and the $2^{-\Delta\Delta CT}$ Method. Methods 2001;25:402–
715 8. doi:10.1006/meth.2001.1262.
- 716 [31] Fulcher LJ, He Z, Mei L, Macartney TJ, Wood NT, Prescott AR, et al. FAM83D
717 directs protein kinase CK1 α to the mitotic spindle for proper spindle
718 positioning. EMBO Rep 2019:e47495. doi:10.15252/embr.201847495.
- 719 [32] Waters AM, Ozkan-Dagliyan I, Vaseva A V, Fer N, Strathern LA, Hobbs GA, et
720 al. Evaluation of the selectivity and sensitivity of isoform- and mutation-specific
721 RAS antibodies. Sci Signal 2017;10:eaa03332. doi:10.1126/scisignal.aao3332.

- 722 [33] Reynolds AB, Daniel J, Mccrea PD, Wheelock MJ, Wu J, Zhang Z.
723 Identification of a New Catenin: the Tyrosine Kinase Substrate p120cas
724 Associates with E-Cadherin Complexes. *Mol Cell Biol* 1994;14:8333–42.
- 725 [34] Schatz G, Butow RA. How Are Proteins Imported into Mitochondria? *Cell*
726 1983;32:316–8.
- 727 [35] Yu F, White SB, Zhao Q, Lee FS. HIF-1alpha binding to VHL is regulated by
728 stimulus-sensitive proline hydroxylation. *Proc Natl Acad Sci U S A*
729 2001;98:9630–5. doi:10.1073/pnas.181341498.
- 730 [36] Spencer-Smith R, Koide A, Zhou Y, Eguchi RR, Sha F, Gajwani P, et al.
731 Inhibition of RAS function through targeting an allosteric regulatory site. *Nat*
732 *Chem Biol* 2017;13:62–8. doi:10.1038/nchembio.2231.
- 733 [37] Morandi L, de Biase D, Visani M, Cesari V, De Maglio G, Pizzolitto S, et al.
734 Allele Specific Locked Nucleic Acid Quantitative PCR (ASLNAqPCR): An
735 Accurate and Cost-Effective Assay to Diagnose and Quantify KRAS and BRAF
736 Mutation. *PLoS One* 2012;7:e36084. doi:10.1371/journal.pone.0036084.
- 737 [38] Tan YH, Liu Y, Eu KW, Ang PW, Li WQ, Tellez MS, et al. Detection of BRAF
738 V600E mutation by pyrosequencing. *Pathology* 2008;40:295–8.
739 doi:10.1080/00313020801911512.
- 740 [39] Cox AD, Der CJ. Ras history: The saga continues. *Small GTPases* 2010;1:2–
741 27. doi:10.4161/sgtp.1.1.12178.
- 742 [40] Janes MR, Zhang J, Li L-S, Hansen R, Peters U, Guo X, et al. Targeting KRAS
743 Mutant Cancers with a Covalent G12C-Specific Inhibitor. *Cell* 2018;172:578–
744 89. doi:10.1016/j.cell.2018.01.006.
- 745 [41] Patricelli MP, Janes MR, Li L-S, Hansen R, Peters U, Kessler L V, et al.
746 Selective Inhibition of Oncogenic KRAS Output with Small Molecules Targeting

- 747 the Inactive State. *Cancer Discov* 2016;6:316–29. doi:10.1158/2159-8290.CD-
748 15-1105.
- 749 [42] McCarthy MJ, Pagba C V., Prakash P, Naji AK, van der Hoeven D, Liang H, et
750 al. Discovery of High-Affinity Noncovalent Allosteric KRAS Inhibitors That
751 Disrupt Effector Binding. *ACS Omega* 2019;4:2921–30.
752 doi:10.1021/acsomega.8b03308.
- 753 [43] Kessler D, Gmachl M, Mantoulidis A, Martin LJ, Zoepfel A, Mayer M, et al.
754 Drugging an undruggable pocket on KRAS. *Proc Natl Acad Sci*
755 2019;116:15823–9. doi:10.1073/pnas.1904529116.
- 756 [44] Lindsay CR, Blackhall FH. Direct Ras G12C inhibitors: crossing the rubicon. *Br*
757 *J Cancer* 2019;121:197–8. doi:10.1038/s41416-019-0499-1.
- 758 [45] Guillard S, Kolasinska-Zwierz P, Debreczeni J, Breed J, Zhang J, Bery N, et al.
759 Structural and functional characterization of a DARPin which inhibits Ras
760 nucleotide exchange. *Nat Commun* 2017;8:16111. doi:10.1038/ncomms16111.
- 761 [46] Spencer-Smith R, Li L, Prasad S, Koide A, Koide S, O'Bryan JP. Targeting the
762 $\alpha 4$ - $\alpha 5$ interface of RAS results in multiple levels of inhibition. *Small GTPases*
763 2017;1248:1–10. doi:10.1080/21541248.2017.1333188.
- 764 [47] Koide A, Bailey CW, Huang X, Koide S. The fibronectin type III domain as a
765 scaffold for novel binding proteins. *J Mol Biol* 1998;284:1141–51.
766 doi:10.1006/JMBI.1998.2238.
- 767 [48] Khan I, Spencer-Smith R, O'Bryan JP. Targeting the $\alpha 4$ - $\alpha 5$ dimerization
768 interface of K-RAS inhibits tumor formation in vivo. *Oncogene* 2019;38:2984–
769 93. doi:10.1038/s41388-018-0636-y.
- 770 [49] Tsai FD, Lopes MS, Zhou M, Court H, Ponce O, Fiordalisi JJ, et al. K-Ras4A
771 splice variant is widely expressed in cancer and uses a hybrid membrane-

- 772 targeting motif. Proc Natl Acad Sci 2015;112:779–84.
773 doi:10.1073/pnas.1412811112.
- 774 [50] Schmick M, Vartak N, Papke B, Kovacevic M, Truxius DC, Rossmannek L, et
775 al. KRas Localizes to the Plasma Membrane by Spatial Cycles of
776 Solubilization, Trapping and Vesicular Transport. Cell 2014;157:459–71.
777 doi:10.1016/j.cell.2014.02.051.
- 778 [51] Hu Y, Lu W, Chen G, Wang P, Chen Z, Zhou Y, et al. K-ras G12V
779 transformation leads to mitochondrial dysfunction and a metabolic switch from
780 oxidative phosphorylation to glycolysis. Cell Res 2012;22:399–412.
781 doi:10.1038/cr.2011.145.
- 782 [52] Goodwin JS, Drake KR, Rogers C, Wright L, Lippincott-Schwartz J, Philips
783 MR, et al. Depalmitoylated Ras traffics to and from the Golgi complex via a
784 nonvesicular pathway. J Cell Biol 2005;170:261–72.
785 doi:10.1083/jcb.200502063.
- 786 [53] Symonds JM, Ohm AM, Tan A-C, Reyland ME. PKC δ regulates integrin α V β 3
787 expression and transformed growth of K-ras dependent lung cancer cells.
788 Oncotarget 2016;7:17905–19. doi:10.18632/oncotarget.7560.
- 789 [54] Singh A, Greninger P, Rhodes D, Koopman L, Violette S, Bardeesy N, et al. A
790 Gene Expression Signature Associated with “K-Ras Addiction” Reveals
791 Regulators of EMT and Tumor Cell Survival. Cancer Cell 2009;15:489–500.
792 doi:10.1016/j.ccr.2009.03.022.
- 793 [55] Singh A, Sweeney MF, Yu M, Burger A, Greninger P, Benes C, et al. TAK1
794 Inhibition Promotes Apoptosis in KRAS-Dependent Colon Cancers. Cell
795 2012;148:639–50. doi:10.1016/j.cell.2011.12.033.
796

797

798

799 **Figure Legends**

800

801 **Figure 1 – Generation of GFP-KRAS knockin in A549 NSCLC cells by**
802 **CRISPR/Cas9.**

803 (A) Sequence Alignment of RAS protein isoforms K-RAS4A (Uniprot-ID: P01116-1),
804 K-RAS4B (P01116-2), H-RAS (P01112-1) and N-RAS (P01111-1). Degrees of
805 shading according to % sequence identity between the four proteins. Asterisk denotes
806 frequently mutated G12 position. (B) A549 WT or K-RAS_{GFP/GFP} knock-in (KI; hereafter
807 called A549_{GFPKRAS}) cell lysates were separated by SDS PAGE and the indicated
808 antibodies were used for detection by Western blotting. Arrows indicate different RAS
809 species (black: endogenous K-RAS; dark grey: GFP-K-RAS; light grey: H-/N-RAS).
810 (C) Lysates were processed as in (B) and subjected to immunoprecipitation with GFP-
811 trap beads. I = Input, Ft = Flowthrough, E = Elution. (D) Widefield immunofluorescence
812 microscopy of untreated A549_{GFPKRAS} cells labelled with antibodies specific for GFP
813 (all left panels, cyan) and P120 (top two middle panels, magenta) or ATPB (bottom
814 two middle panels, magenta), and DAPI (all left and middle panels, blue). Overlay of
815 GFP and P120/ATPB is shown on the right. Scalebar = 10µm. Two representative
816 images for each staining are shown. All blots are representative of at least 3
817 independent experiments.

818

819

820 **Figure 2 – AdPROM mediated degradation of GFP-K-RAS**

821 (A) Schematic representation of the proteolytic AdPROM system. The high affinity

822 GFP-binder aGFP16 is fused to VHL, which is recruited by EloB and EloC to Cul2.
823 aGFP16 recruits GFP-tagged K-RAS and presents it in close proximity to RBX1 in
824 the assembled Cul2 complex. Ubiquitin (Ub) is transferred onto K-RAS, which is
825 subsequently degraded (dashed lines and faded). (B) After treatment with
826 retroviruses and selection, cell lysates of indicated cell lines were separated on SDS
827 PAGE and analysed by Western blotting using the indicated antibodies. (C) Indicated
828 cell lines were treated with 1 μ M MLN4924 in 0.1% DMSO, or just DMSO at 0.1%
829 for 24 h. Samples were further processed as in (B). (D) Indicated cell lines were
830 analysed on a Canto flow cytometer. Shown populations were preselected for cells
831 and single cells before defining the gate for GFP positive cells (shown). GFP-A is
832 plotted against PE-A in all cases. Numbers indicate percentage of cells within the
833 respective gate. (E) Histogram representation of plots in (D). KI = A549 KRAS^{GFP/GFP}
834 cells (referred to as a549^{GFPKRAS} cells throughout text). Western blots are
835 representative of at least 3 independent experiments. Flow cytometry data are
836 representative of 2 independent experiments.

837

838 **Figure 3 – Degradation of endogenous RAS using a RAS-specific antibody.**

839 (A) Cell lysates of indicated cell lines were subjected to immunoprecipitation with
840 anti-Flag beads. Input (I), Flowthrough (Ft) and precipitates (IP) were run on SDS-
841 PAGE and subjected to Western blotting with the respective antibodies. (B), (C) and
842 (G) SDS-PAGE and Western blots of lysates of indicated cell lines using the
843 indicated antibodies. Samples were treated with 1 μ M MLN4924 or 0.1% DMSO for
844 24 h (C). (D) and (E), flow cytometric analysis of indicated cells, done as in Figure 2.
845 KI = A549^{GFPKRAS} cells. (F) Widefield immunofluorescence microscopy of indicated
846 cell lines treated with anti-GFP antibody and DAPI for staining. Scalebar = 10 μ m.

847 Two representative images are shown for each condition. (H) 5,000 cells from (B)
848 and (G) were grown in triplicate in 12 well dishes. After 7 days, cells were fixed and
849 stained with crystal violet. A representative image of the replicates is shown. (I)
850 Staining from plates in (H) was extracted by methanol and absorbance at 570 nm
851 was measured. Plotted 570 nm values are relative to the respective untreated
852 sample. The number of biological replicates is indicated next to the cell line name.
853 For statistical analysis, one-way ANOVA analysis with Dunnett's multiple
854 comparisons test was done. Comparisons were drawn to the untreated sample.
855 Western blots and immunofluorescence data are representative of at least 3
856 independent experiments. Flow cytometry data are representative of 2 independent
857 experiments.

858

859 **Figure 4 – Degradation of RAS in different cell lines and effects on proliferation**

860 Lysates of untreated (A), or retrovirally transduced cell lines (indicated expression
861 constructs) (B) were separated by SDS PAGE and analysed by Western blotting with
862 the indicated antibodies. Comparison of cell lines in (A) was done only once. K-RAS
863 mutation statuses for individual cell lines are indicated in brackets. (C) 5,000 cells from
864 (B) were grown in triplicate in 12-well dishes. After 7 days, cells were fixed and stained
865 with crystal violet. A representative image of the replicates is shown. (D) Staining from
866 plates in (C) was extracted by methanol and absorbance at 570 nm was measured.
867 Plotted 570 nm values are relative to the respective untreated sample. The number of
868 biological replicates (applies to Western blots in (B) as well) is indicated next to the
869 cell line. For statistical analysis one-way ANOVA analysis with Dunnett's multiple
870 comparisons test was done. Comparisons were drawn to the untreated sample.

A

*

```

K-RAS4A 1 MTEYKLVVVGAGGVGKSALTIQLIQNHFYDEYDPTIEDSYRKQVVIDGETCLLDILDTAGQE 64
K-RAS4B 1 MTEYKLVVVGAGGVGKSALTIQLIQNHFYDEYDPTIEDSYRKQVVIDGETCLLDILDTAGQE 64
H-RAS 1 MTEYKLVVVGAGGVGKSALTIQLIQNHFYDEYDPTIEDSYRKQVVIDGETCLLDILDTAGQE 64
N-RAS 1 MTEYKLVVVGAGGVGKSALTIQLIQNHFYDEYDPTIEDSYRKQVVIDGETCLLDILDTAGQE 64

K-RAS4A 65 SAMRDQYMRGTGEGFLCVFAINNTKSFEDIHHYREQIKRVKDSDDVPMVLVGNKCDLPSRTVDTK 128
K-RAS4B 65 SAMRDQYMRGTGEGFLCVFAINNTKSFEDIHHYREQIKRVKDSDDVPMVLVGNKCDLPSRTVDTK 128
H-RAS 65 SAMRDQYMRGTGEGFLCVFAINNTKSFEDIHHYREQIKRVKDSDDVPMVLVGNKCDLAARTVESR 128
N-RAS 65 SAMRDQYMRGTGEGFLCVFAINNSKSFADINLYREQIKRVKDSDDVPMVLVGNKCDLPTRTVDTK 128

K-RAS4A 129 QAQDLARSYGIPPIETSAKTRQGVDAFYTLVREIRQYRLKKISKE-EKTPGCVKIKKCIIM 189
K-RAS4B 129 QAQDLARSYGIPPIETSAKTRQGVDAFYTLVREIRKHKCKM-SKD-GKKKKKSKTKCVIM 188
H-RAS 129 QAQDLARSYGIPPIETSAKTRQGVDAFYTLVREIRQHKLRKLNPPDESGPGCMSCK-CVLS 189
N-RAS 129 QAHELAKSYGIPPIETSAKTRQGVDAFYTLVREIRQYRMKKLNSDDGTQGCMLP-CVVM 189

```

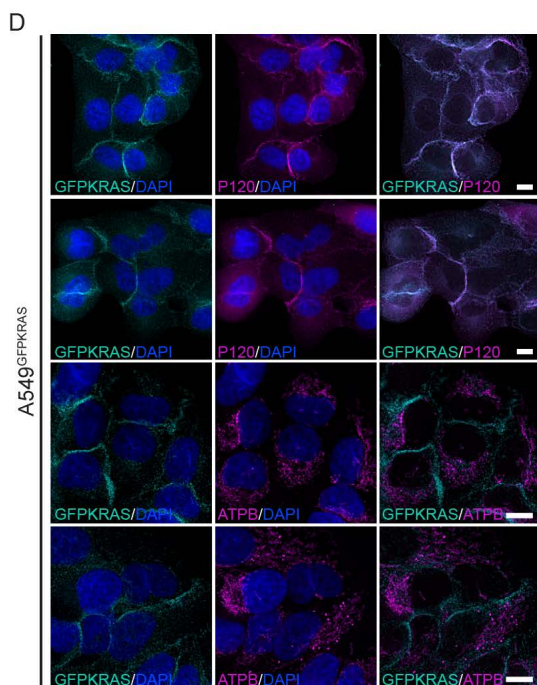
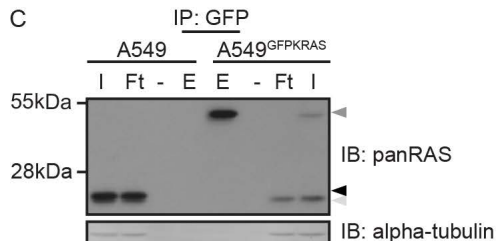
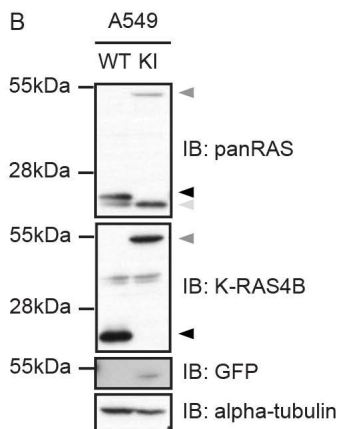


Figure 1 - Generation of GFP-KRAS knockin in A549 NSCLC cells by CRISPR/Cas9.

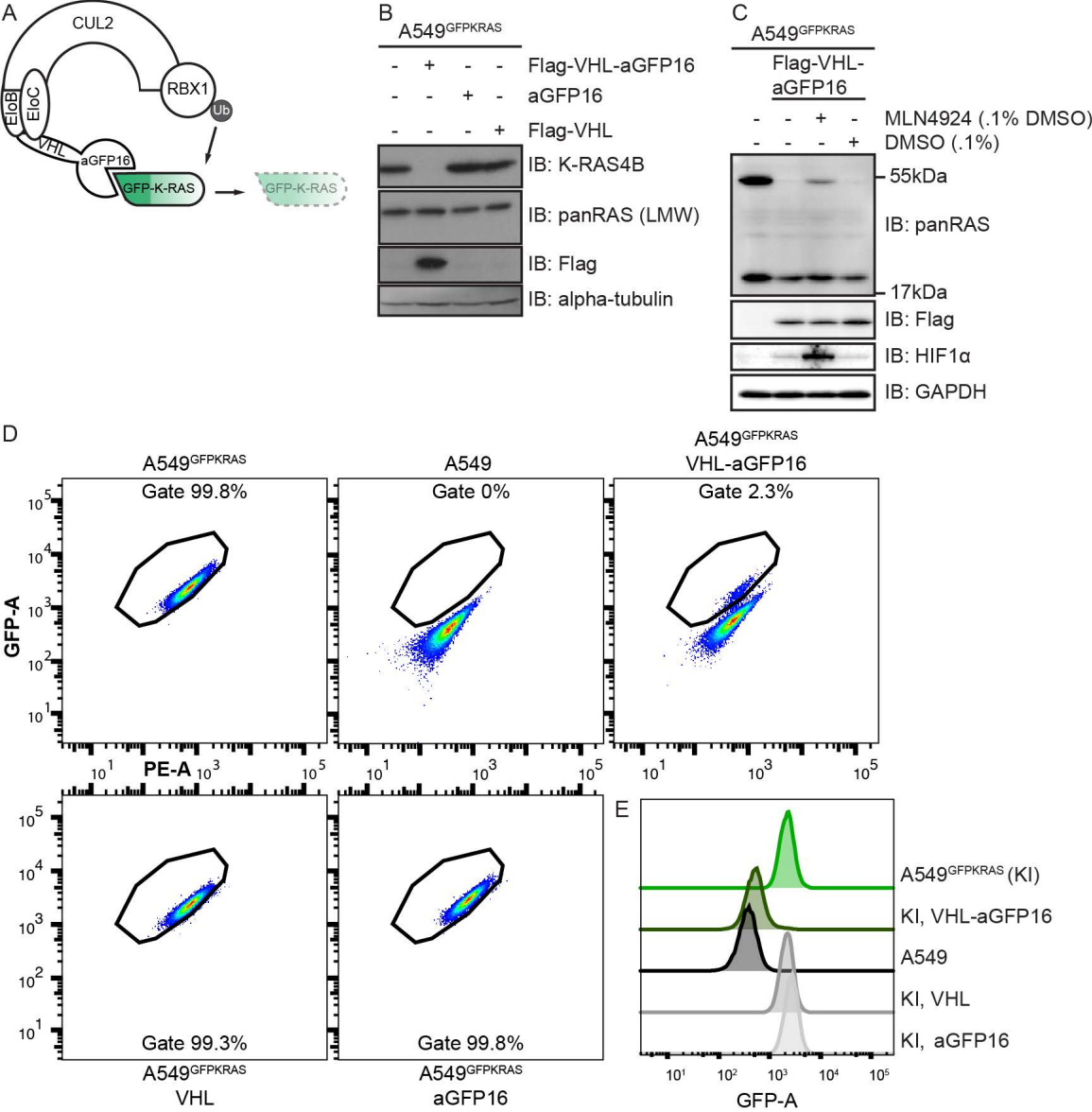


Figure 2 – AdPROM mediated degradation of GFP-K-RAS

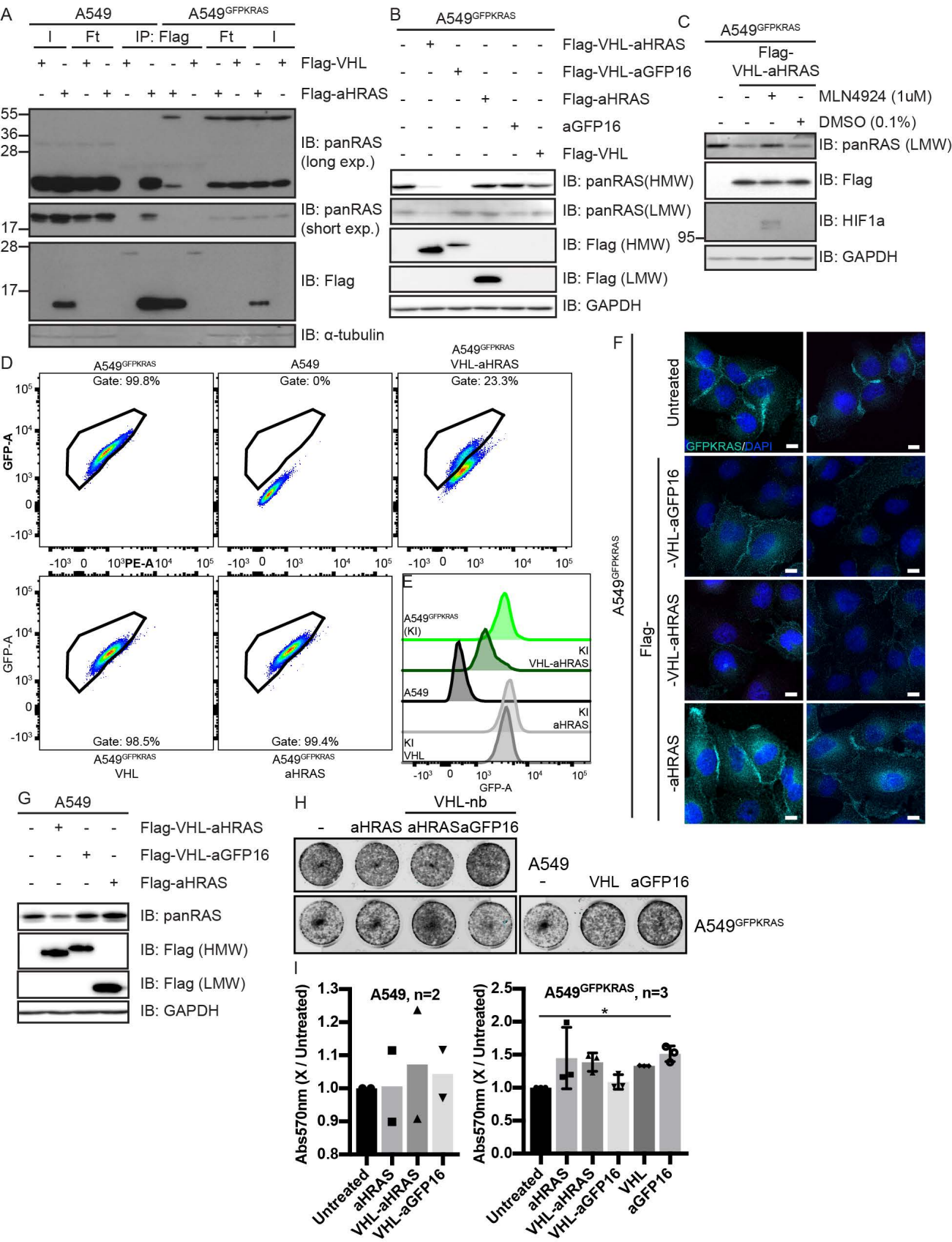


Figure 3 - Degradation of endogenous RAS using a RAS-specific monobody.

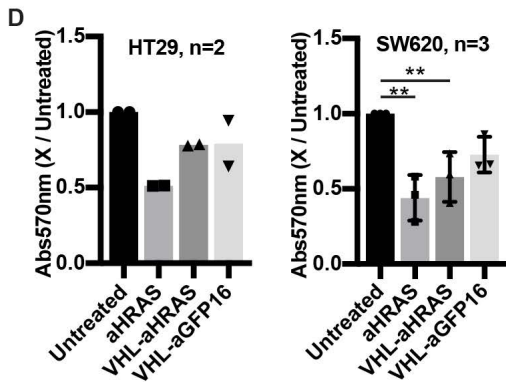
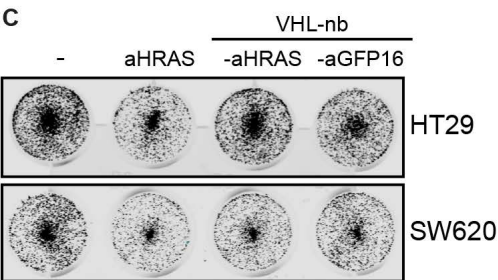
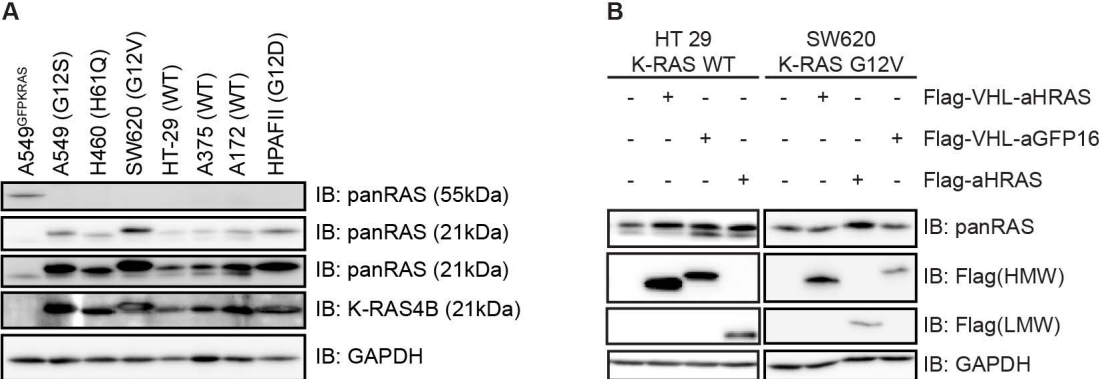


Figure 4 - Degradation of RAS in different cell lines and effects on proliferation

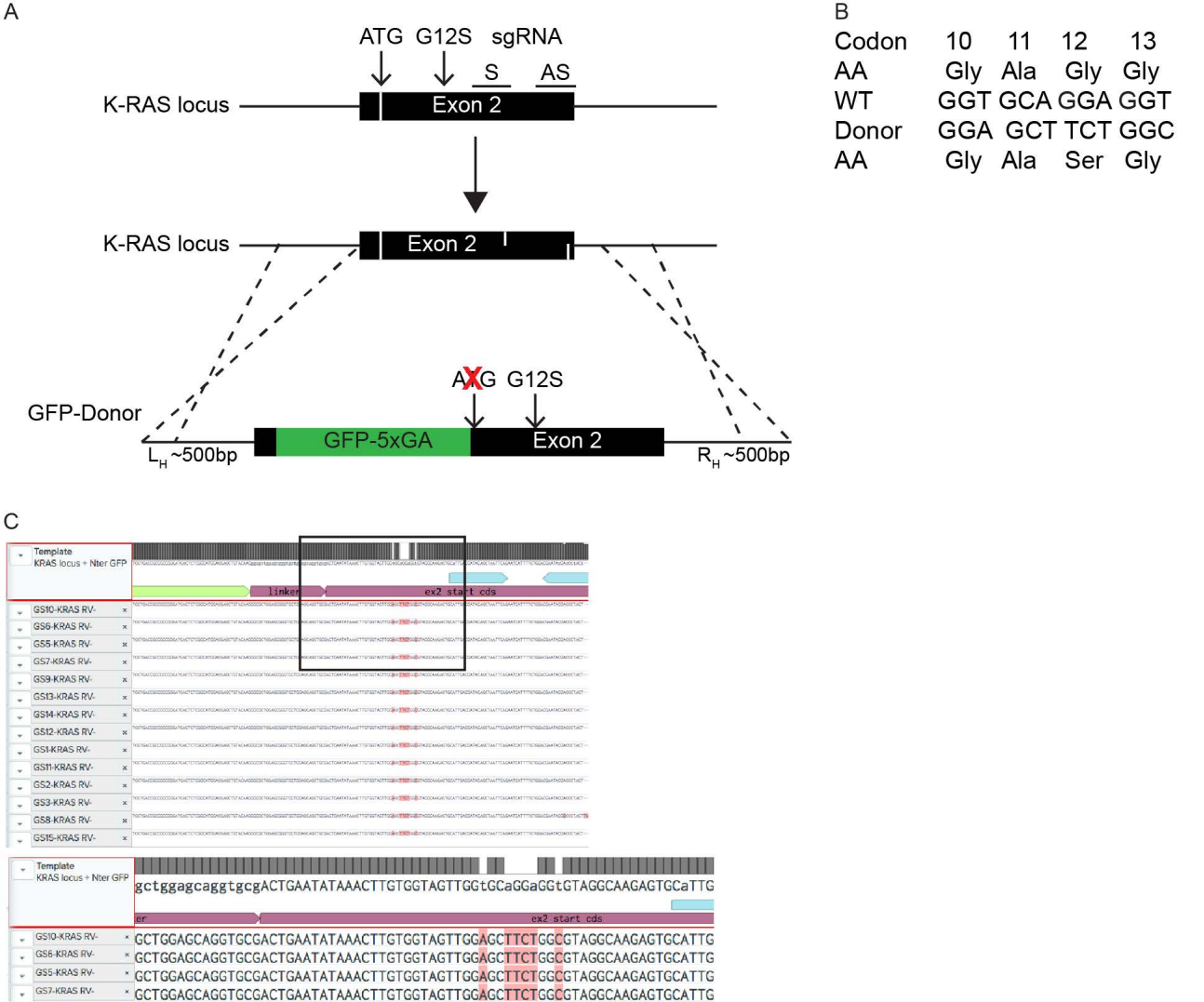


Figure S1 - Characterization of A549^{GFPKRAS}

(A) Schematic representation of the CRISPR/Cas9 strategy used for A549 cells. Two plasmids encoding sgRNA sequences targeting the K-RAS locus on exon 2 were co-expressed with Cas9-D10A, to create two nicks in K-RAS complementary strands for a double stranded break. A donor plasmid consisting of GFP cDNA sequence without the stop codon followed by a GAGAGAGAGA linker flanked by Left and Right homology arms (L_H and R_H , respectively) was designed and co-transfected to allow homologous recombination for insertion of the GFP-5xGA tag onto the native K-RAS locus at the start codon. Consequently, the start codon of K-RAS was eliminated. (B) The indicated silent mutations on sgRNA target codons (10-13) were introduced in the donor sequence to block subsequent dsDNA breaks following integration of the donor on K-RAS locus. (C) A screenshot of DNA sequence analysis from Benchling of the resulting GFP-positive clone. Top: 14 DNA sequence files were aligned against the predicted WT RAS gene locus sequence with the GFP-fusion (indicated in light green) and the 5xGA linker. The box indicates area of the image that is magnified below. The magnified area shows DNA sequence alignment of the A549^{GFPKRAS} cell line at the site of the G12S mutation, which also shows silent mutations. The Ab1 files containing the DNA sequence chromatograms are deposited online.

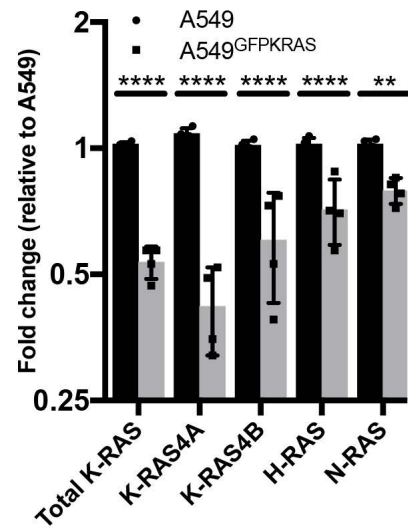


Figure S2 - Analysis of RAS transcript levels in A549 WT and A549^{GFPKRAS}

mRNA was extracted from indicated cell lines and cDNA was synthesised. Fold changes in RAS expression were calculated after qRT-PCR with specific primers between A549^{GFPKRAS} (grey bars) and A549 WT (black bars). Error bars are shown for n=4. Statistical significance was calculated with a 2-way ANOVA, Sidak's multiple comparison test.

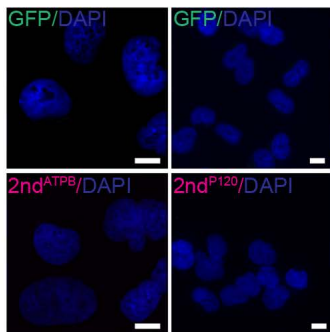


Figure S3 - Negative controls for Figure 1D

Experimental procedure is described in Figure 1D. An additional slide of A549 WT cells (GFP negative) was treated with the secondary antibody used for ATPB or P120. Exposure times are set to be the same as for the positive sample slides in Figure 1D. Scalebar = 10 μ m

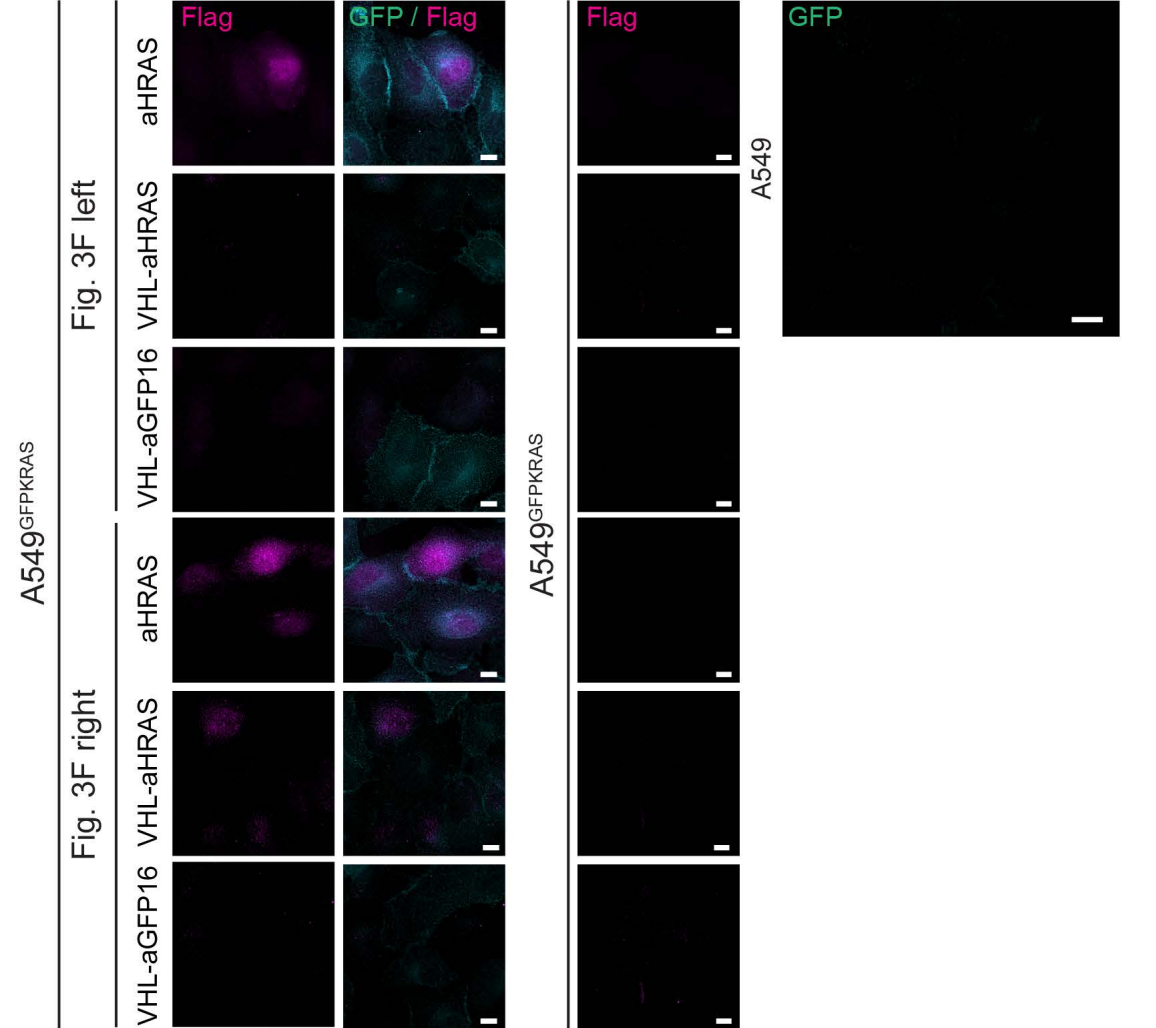


Figure S4 - FLAG signal and controls for Figure 3F.

Slides of Fig. 3F (A549^{GFPKRAS} with or without indicated transductions) were additionally stained with anti-FLAG antibody and secondary stain for detection in the 594 channel (Flag) (2 leftmost columns). The top 4 rows represent the left column of Fig. 3F, the bottom 4 rows the right column of Fig. 3F. Appropriate negative control (A549^{GFPKRAS} cells without a FLAG construct) were stained with the same antibody combination and exposure time (Column 3). Brightness and contrast for individual positive stains were background adjusted for these samples (note that the same negative sample is used for more than one picture). Additionally A549 WT cells were stained with the GFP antibody to act as negative control for GFP signal in main Figure 3F (panel on the right). Scalebar = 10µm.